Full length article

Stabilization of high-pressure phase of CdO by nanoparticle formation in $Cd_xZn_{1-x}O$ thin films

Arkaprava Das [a,*], Camille Latouche [b,c], Stephane Jobic [b], Eric Gautron [b], Amina Merabet [b], Marcin Zajac [d], Akinori Shibui [e], Peter Krüger [e], Wei-Hsiang Huang [f], Chi-Liang Chen [f], Asokan Kandasami [g], Carla Bittencourt [a]

[a] Chimie des Interaction Plasma surface, University of Mons, Mons, Belgium
[b] Nantes Université, CNRS, Institut des Matériaux de Nantes Jean Rouxel, IMN, Nantes F-44000, France
[c] Institut Universitaire de France, Paris 75005, France
[d] SOLARIS National Synchrotron Radiation Centre, Jagiellonian University, Krakow, Poland
[e] Graduate School of Science and Engineering, Chiba University, Chiba, Japan
[f] National Synchrotron Radiation Research Center, Hsinchu, Taiwan
[g] Department of Physics & Centre for Interdisciplinary Research, University of Petroleum and Energy Studies (UPES) Dehradun, India

ARTICLE INFO

ABSTRACT

We report the observation of the high-pressure B2 phase in CdO nanoparticles obtained by temperature induced phase transition from the CdO B1 phase in $Cd_xZn_{1-x}O$ films grown on a Si substrate. The structural transformation occurs upon annealing the film from 700 to 900 °C and is monitored by X-ray diffraction and Raman spectroscopy. Concomitantly, willemite Zn_2SiO_4 nanoparticles form at the $Cd_xZn_{1-x}O$/Si interface and are evidenced using scanning transmission electron microscopy, X-ray absorption and photoelectron spectroscopies. The presence of Zn_2SiO_4 at the film-substrate interface is assumed to exert locally a high pressure on the CdO crystallites. The B1 to B2 phase transition in CdO was previously only reported under hydrostatic pressure conditions. By varying the Cd content and adjusting the growth conditions, we have succeeded in stabilizing the metastable B2 phase under ambient conditions, which holds significant potential for applications in energy storage and stress sensing.

1. Introduction

Semiconductors have played a crucial role in the development of novel technologies over the last century. Among them, transparent conducting wurtzite oxide Zinc oxide (WZ) (ZnO) has garnered significant attention due to its wide direct bandgap (3.37 eV) and a high exciton binding energy (60 meV) compared to the thermal energy at RT (25 meV). Numerous studies have explored the different possible applications of ZnO, including its use as a pigment for anti-pathogenic coatings [1], piezoelectric devices [2], acoustic wave transducers [3], and active layers in chemical sensors [4]. Similarly, CdO (rock-salt (B1) structure type, RS) is a wide band gap (2.2 eV) semiconductor oxide that is recognized for its high electrical conductivity ($>10^{14}$ S/cm) and high electron mobility (>100 cm^2/V/s) [5–7]. Consequently, Cd has been identified as a key doping material to enhance the optoelectronic properties of ZnO. The incorporation of cadmium (Cd) into ZnO

effectively narrows the bandgap, rendering the optoelectronic device suitable for operation in the visible region [8–10].

The mixing of RS CdO and WZ ZnO would result in the formation of mixed binary oxide [11]. However, obtaining a single crystallographic phase in $Cd_xZn_{1-x}O$ thin films under normal growth conditions in the mid-composition region is challenging as CdO and ZnO crystallize in the RS and WZ phases, respectively. Additionally, the uniform mixing between CdO and ZnO is further impeded by the low atomic solubility (< 2 %) of Cd in WZ ZnO) [12,13]. To overcome the miscibility limitation, researchers have endeavored to synthesize $Cd_xZn_{1-x}O$ binary oxide with high Cd concentration using different non-equilibrium growth methods. The synthesis of WZ $Cd_xZn_{1-x}O$ thin films, where the band gap varies from 3.2 to 1.8 eV, are reported for x up to 0.7 using the remote plasma enhanced metal organic chemical vapour deposition [14,15]. Using the pulsed filtered cathodic arc deposition (PFCAD) method, $Cd_xZn_{1-x}O$ mixed binary oxide for $x < 0.67$ were obtained with high free electron

* Corresponding author.
E-mail address: arkaprava.das@umons.ac.be (A. Das).

concentration (from mid-10^{19} to $>10^{20}$/cc) due to native defects and appreciable mobility value ($\sim$20 cm^{2}V^{-1}S^{-1}) [16]. For DC magnetron sputtering Cd$_x$Zn$_{1-x}$O thin film deposition, the dominance of the WZ phase is observed for x up to 0.66 [17]. Therefore, we have focused on the study of Cd$_x$Zn$_{1-x}$O thin films in mid-composition (i.e., $x = 0.4$) synthesized by the sol-gel method. To obtain high nano-crystalline thin films, high-temperature annealing was used. Despite significant challenges, the crystallographic phase identification demonstrated the presence of RS CdO (B1) and a remarkable phase transformation (PT) from the CdO B1 (NaCl) to CdO B2 (CsCl) structural phase within the thin film as the post-synthesis annealing temperature increased. This observation has prompted us to investigate the B1 to B2 type phase transformation mechanism. Notably, this phenomenon has only been reported using the diamond anvil cell (DAC) technique [18].

Theoretical modelling has demonstrated that 4d CdO and 3d ZnO transition metal oxides can suffer a B1 to B2 type PT at 89 GPa and 256 GPa, respectively [19,20]. These pressure values are challenging to obtain experimentally. Therefore, only one experimental report is available for CdO with B1 to B2 type PT [18], and for ZnO, no experimental evidence is available to our knowledge. Such theoretically predicted critical pressure (P$_{TC}$) values for PT are questionable as relativistic corrections, nonzero temperature, and zero-point motion can alter such predictions. Therefore, precise diffraction measurements are essential to understand the B1 to B2 PT kinetics. Apart from Liu *et al.* in 2004, such investigation is yet to be done due to experimental limitations in kinetically achieving the B2 phase in CdO [18]. Wurtzite to rocksalt PT with $\sim$9 GPa pressure in ZnO bulk has been reported elsewhere [21], and with compositional variation for $x>0.67$ in Cd$_x$Zn$_{1-x}$O thin films [8]. So, the wurtzite to rocksalt PT has been reported for undoped ZnO and for Cd$_x$Zn$_{1-x}$O ($x>0.67$) binary oxides as for these materials it requires $<$15 GPa pressure. However, using in situ high-pressure angle dispersive synchrotron X-ray diffraction technique, Liu *et al.* showed the B1 to B2 type PT for bulk CdO which requires beyond 90 GPa pressure. [18]. Investigating the electronic structure and microscopic properties of a kinetically stable B2 phase under ambient conditions is a complex task that typically requires high-pressure techniques such as the diamond anvil cell (DAC). Currently, only a small amount of research has been conducted in this field.

In our current study of the Cd$_x$Zn$_{1-x}$O ($x = 0.4$) thin film, we have successfully achieved a kinetically stable B2 phase without using the diamond anvil cell (DAC) technique. Through local pressure generation in the thin film, we have attained a thermodynamically stable B2 phase at room temperature and pressure. This breakthrough has enabled us to investigate the modifications in electronic structure and changes in microscopic properties during the B1 to B2 type phase transition in the Cd$_x$Zn$_{1-x}$O ($x = 0.4$) thin film. The primary goal of this research is to uncover the underlying source of the local pressure generation within the lattice that triggers this PT. Ultimately, our findings on the correlation between the phase transition, microscopic and electronic properties will be valuable in understanding the fundamental physiochemical interactions that play a crucial role in energy storage and stress sensing [8].

2. Experimental methods

The thin films of ZnO with 40 % Cd concentration were prepared with the sol-gel chemical synthesis method using a spin coater. The detailed process is described elsewhere [22]. The post synthesis annealing was done in a tubular furnace for 700 °C, 800 °C, 850 °C, and 900 °C in a flowing oxygen environment. The "Cd$_x$Zn$_{1-x}$O" thin films annealed at these different temperatures are named CZ700, CZ800, CZ850, and CZ900, respectively. ZnO thin films used as references were annealed at 700 °C, 800 °C, and 900 °C. They are named Z700, Z800, and Z900, respectively.

X-ray diffraction (XRD) measurements were performed with a Bruker High-resolution X-ray diffractometer system using a Cu K_α beam. Raman

Spectroscopic measurements have been accomplished at RT with a SENTERRA spectrometer (Bruker) using an Ar ion laser (532 nm) with 0.2 mW laser operating power. Scanning Electron Microscopy (SEM) measurements have been performed with a SU8020 HITACHI model with a 3.0 keV electron beam energy. Topographical measurements were performed using the Atomic Force Microscopy (AFM) technique using NANOSCOPE II tapping mode. The microstructure was characterized using a Cs probe corrected STEM Themis Z G3 (Thermo Fisher Scientific) equipped with a High Angle Annular Dark Field (HAADF) detector (Fischione) operating at 300 kV accelerating voltage, with a 31 mrad convergence angle and 63–200 mrad collection angle. It is equipped with the 4-SDD detectors Super-X system, allowing EDS analysis. Cross sections of the samples were prepared using a focused ion beam (FIB) (ZEISS Crossbeam 550 L). Pt/C layers were deposited on top of the samples before FIB milling to protect them. Surface chemical states were investigated with an ESCA-5000 (Physical Electronics) Versa Probe system using an Al K_α (1486.7 eV) beam attached to a 124 mm hemispherical electron analyzer. Calibration during XPS measurements was done using C 1 s edge (284.6 eV). X-ray absorption near edge spectroscopic (XANES) measurements have been performed for Zn $L_{2,3}$ and O K edges in total electron yield (TEY) detection mode at PIRX beamline [23] in the SOLARIS synchrotron, Poland [24]. Extended X-ray absorption fine structure (EXAFS) data for the Zn K edge has been recorded in fluorescence detection mode at the TPS 44A beamline, National Synchrotron Radiation Research Center (NSRRC), Taiwan.

2.1. Computational methods

The density of states (DOS) calculation for the Cd$_x$Zn$_{1-x}$O ($0 \leq x \leq 1$) system is performed with projected augmented wave (PAW) method using Vienna *Ab Initio* simulation package (VASP) software [25,26]. $12 \times 12 \times 6$ Monkhorst-pack k-mesh sampling has been used to optimize the geometries [27]. The kinetic energy cut-off of the plane wave basis was set at 540 eV. The total energy convergence criterion for self-consistent field cycles was 10^{-5} eV. The PyDEF software was used to realize the graphical representation of the DOS [28,29]. The Zn L-edge absorption spectra were computed in supercells of at least 64 atoms using the so-called final state approximation, i.e., with a full core hole on one Zn site. The energy splitting between the 2$p_{3/2}$ and 2$p_{1/2}$ core levels was taken from photoemission data (23.3 eV). The L_3 and L_2 edge spectra were added in the statistical branching ratio 2:1. Since absolute binding energies are difficult to reproduce in DFT, we have shifted the spectra rigidly to align the L_3-edge with the experiment.

3. Results and discussion

3.1. Crystallographic phase identification

Fig. 1(a) shows the X-ray diffractograms (XRD) for the annealed thin films. The Bragg reflections for the wurtzite ZnO (*space group P6_3mc*) and the CdO rocksalt phases are indexed in Fig. 1(a). For the CZ700 thin film, B1 phase peaks, i.e., for CdO rocksalt phase (*space group Fm-3 m*), are situated at 33.0° (111) and 38.3° (200). The reflections for the wurtzite phase (*space group P6_3mc*) are situated at 31.6° (100), 34.3° (002), 36.1° (101), 47.4° (102). Therefore, the CZ700 thin film consists of a mixed phase containing ZnO wurtzite and CdO rocksalt crystallites [30]. A gradual evolution of the peak at 32° is observed with increasing annealing temperature, indicating the NaCl B1 (*space group Fm-3 m*) to CsCl B2 (*space group Pm-3 m*) phase transition (PT). For the CdO powder, the B1 to B2 PT is reported experimentally [18] and theoretically [20] under hydrostatic pressure. For our Cd$_x$Zn$_{1-x}$O thin film, the complete transition takes place around 900 °C. For the CZ900 thin film, two low-intensity peaks are observed at 38.8°, and 42.1° corresponding to the trigonal (223) and (202) reflections of the willemite Zn$_2$SiO$_4$ phase (*space group R-3*). In the following, it is shown that the formation of the trigonal Zn$_2$SiO$_4$ phase is crucial for the B1 to B2 PT. In Figure S1
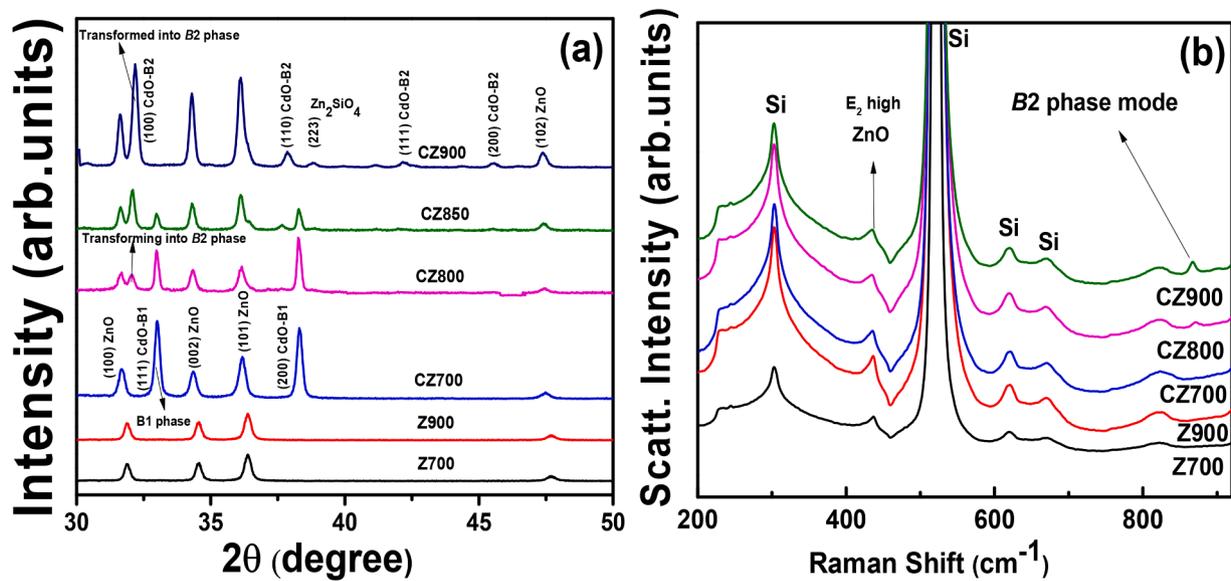
Fig. 1. (a): X-ray diffraction patterns and (b) Raman spectra for ZnO and Cd$_x$Zn$_{1-x}$O ($x = 0.4$) thin films at different annealing temperatures showing $B1$ to $B2$ phase transformation in CdO sublattice.

of SI (Supplementary information file) we have shown the XRD pattern for CZ900 thin films in logarithmic scale where (223) and (202) reflection of willemite trigonal Zn$_2$SiO$_4$ phase is well visible. We have performed the structural Reitveld refinement for Z700, CZ700, and CZ900 thin films. In Figure S2 of SI, the structural refinements for the thin films are stack plotted. The details of the Rietveld refinement, and the calculated structural parameters, are mentioned in Table ST1 of the SI.

The lattice parameter 'a' for hexagonal wurtzite ZnO can be calculated with the following equation [31]:

$$a = \frac{\lambda}{\sqrt{3}\sin\theta} \tag{1}$$

Here θ corresponds to the position of (100) reflection of the wurtzite ZnO phase in the XRD pattern.

From Eq. (1), an increment of ~0.9 % in the 'a' lattice parameter is expected with shifting of 0.2° of (100) reflection of ZnO towards a lower value.

Fig. 1(b) shows the Raman spectra for the Z700, Z900, CZ700, CZ800, and CZ900 thin films. The Raman modes observed at 303 cm^{-1}, 520 cm^{-1}, 620 cm^{-1}, and 671 cm^{-1} correspond to the Si substrate [32]. The mode at 435.5 cm^{-1}, i.e., the E$_2$ (high), indicates the hexagonal wurtzite phase of ZnO. The mode at 867.2 cm^{-1}, is assumed to correspond to the transformed B2 phase, which has yet to be reported in the literature to our knowledge.

3.2. Grain growth mechanism

Fig. 2 displays the SEM images of the Z700, Z800, Z900, and CZ700, CZ800, CZ900 films. The Z700, Z800, and Z900 films show grain growth with increasing annealing temperature due to sintering process. In sintering heat treatment process where loose material is subjected to high
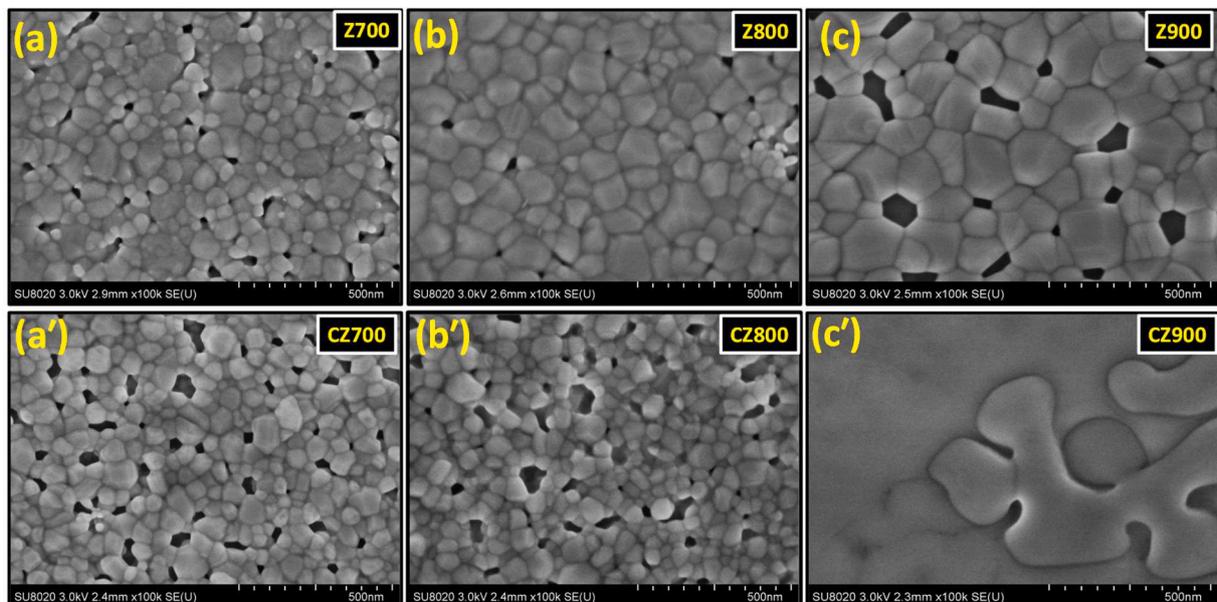
Fig. 2. Scanning electron microscopic images for ZnO (a, b, c) and Cd$_x$Zn$_{1-x}$O ($x = 0.4$) thin films (a', b', c') at 700 °C, 800 °C and 900 °C respectively.

temperature and pressure to compact it into a solid piece. From the observed surface morphology, it is established that there is a homogenous distribution of inter-connected grains with voids. The mean void size increases with increasing annealing temperature as sintering process induced synthesis of compact solid piece of mixed oxide. This happens in Z900 thin film resulting a larger void space among the grains. For the CZ900 thin film, annealed at 900 °C, which is near the melting temperature of CdO (~1000 °C), there is a probability that a portion of the CdO melts and subsequently condensates at energetically favourable sites to minimize the overall surface energy. This would support the formation of larger voids or ribbon-like morphology.

Figure S3 (Supplementary information file) depicts the AFM micrographs for the CZ700, CZ800, and CZ900 thin films. The topographical contrast shows that the local evaporation and agglomeration generated voids. Previously, we have observed such a sheet-like structure for CdO thin films [33]. Brenner *et al.* reported that nanosheet or ribbon-like nanostructure formation is driven by the vapour − solid (VS) process [34]. In the VS process, the vaporization of oxide materials occurs from a high-temperature zone and is further deposited on the surface at a relatively lower temperature region. Similar when the sample is annealed at 900 °C, local CdO evaporation and condensation, along with subsequent nucleation at the energetically favorable site, might have occurred, causing such ribbon-like features.

3.3. Evidence for Zn₂SiO₄ phase formation from soft X-ray photoemission and absorption spectroscopy

3.3.1. XPS analysis

In the XPS survey spectra in addition to the expected elements, i.e., Zn, Cd and O, we observed the silicon for the CZ900 thin film. Fig. 3(a) shows the Cd $3d_{5/2}$ XPS peak corresponding to Cd − O bonding for the CZ700, CZ800 and CZ900 thin films. This peak shifts to higher binding energy for increasing annealing temperature reflecting a change in the chemical environment [33,35]. In Fig. 3(b), a similar shift towards higher BE is observed in the Zn $2p_{3/2}$ peak in the CZ900 sample compared to the CZ700 thin film. While for Z700, Z900, and CZ700 samples the Zn $2p_{3/2}$ peak is centred at 1019.7 eV, indicating no change in the chemical environment of Zn. However, for CZ800 and CZ900 thin films, Zn $2p_{3/2}$ has shifted to 1020.4 eV and 1021.2 eV, respectively. To investigate the chemical structure change for the $Cd_xZn_{1-x}O$ film deposited on Si, the Auger Parameter (*AP*) was calculated using the following equation [36,37].

$$AP = BE(i) + KE(jkl) \qquad (2)$$

In the above equation, $KE(jkl)$ is the kinetic energy of the Auger transition for *jkl* level and $BE(i)$ is the BE of ith electron level. To calculate the Auger Parameter (AP), the position of Zn $L_3M_{45}M_{45}$ (LMM) auger transition peak in the kinetic energy (KE) scale is used (Figure S4 (a)). The position of the Zn $2p_{3/2}$ peak is considered as the BE of the ith electron level. The calculated APs are plotted in Figure S4(b). The calculated AP value for CZ900 is 2009.6 ± 0.1 eV, which agrees with the reported value for willemite Zn₂SiO₄ by Dake *et al.* [38]. As XPS probes the ultimate surface, it suggests that the Zn₂SiO₄ has out-diffused from the film-substrate interface and reached the surface [39,40]. It is expected that Zn₂SiO₄ might have possibly formed in the interface but could not reach up to the surface for Z900 thin film due to the absence of Cd.

Fig. 4(a) shows the Si 2*p* peak for the CZ900, CZ800, CZ700, Z900 and Z700 films. The Si 2*p* peak has closely-shifted spin-orbit components (Δ=0.63 eV), that can be ignored for Si 2*p* peaks from silicon compounds. Therefore, the deconvolution of the Si 2*p* is performed with singlets for the different chemical environment. For the XPS spectrum of the CZ900 film two components were used to reproduce the Si 2*p* peak these are centred at 101.2 eV and at 102.5. The component at 101.2 eV was reported to be associated to Si−O for SiOₓ [41]. The BE value for the Si $2p_{3/2}$ peak for willemite Zn₂SiO₄ is reported between 102.4 − 102.6 eV, which is compatible with our Si 2*p* peak deconvolution for the CZ900 thin film [38]. The deconvolution of Si 2*p* peak evidences the presence of willemite Zn₂SiO₄ at 102.5 eV for CZ900 thin film, whereas there is no signature of the same in the Z900 thin film. A shift of Si 2*p* peak in the CZ900 compared to the CZ700 thin film indicates the formation of Zn₂SiO₄. Such a shift is not observed in Z900 compared to Z700 thin film. The Si 2*p* peak intensity in the absolute scale is almost seven times higher in the CZ900 thin film than in the CZ700 thin film. In Z700, Z900, CZ700 and CZ800, the intensity is relatively small as the thick ZnO film layer has caused the attenuation of the Si signal at the surface.

Fig. 4(b) shows the O 1 s XPS spectra for all thin films. The component centred at 529.2 eV corresponds to the contribution of Zn−O bonding, which does not shift with increasing annealing temperature. The other components centered at 530.5 eV indicate oxygen vacancies (V_O) [33,35,42]. For the CZ700 thin film, three components were used
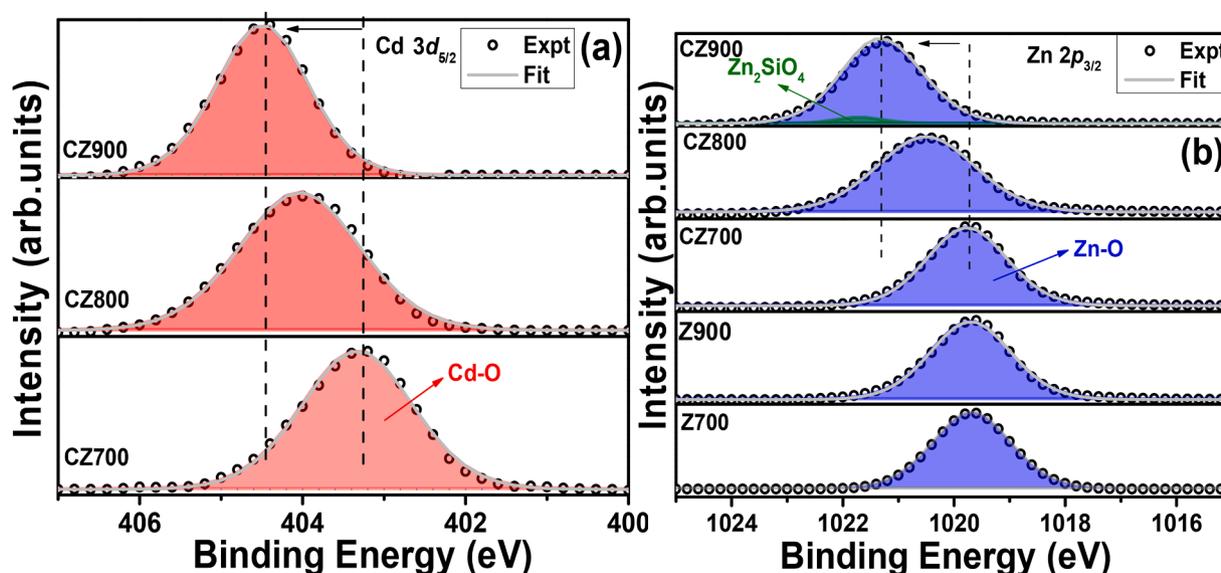
Fig. 3. X-ray photoelectron spectra for Cd 3*d* **(a)** edge for CZ700, CZ800 and CZ900 thin film and Zn 2*p* **(b)** edges for Z700, Z900, CZ700, CZ800 and CZ900 thin films.
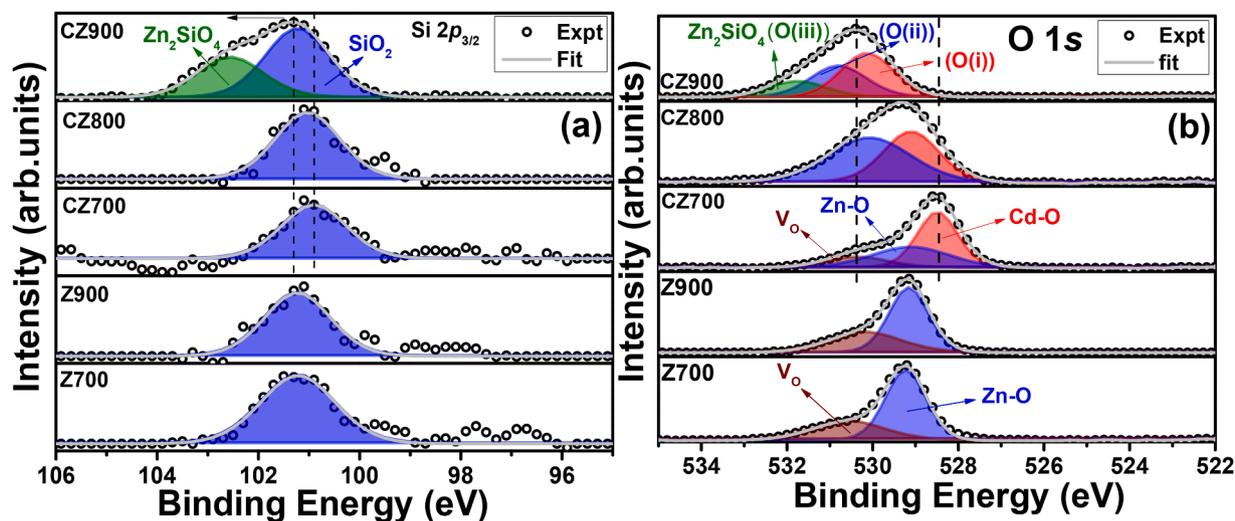
Fig. 4. X-ray photoelectron spectra for Si 2p edges **(a)** and O 1 s edges **(b)** for Z700, Z900, CZ700, CZ800, and CZ900 thin films.

for deconvolution. Components at 528.5 eV and 529.2 eV correspond to Cd − O and Zn − O, respectively, for solgel-derived undoped CdO and ZnO thin films Cd − O and Zn−O peaks are positioned at 528.0 eV and 529.5 eV, respectively [35,43]. For the CZ800 thin film, using two components, i.e., Zn − O, and Cd − O provides a good fitting without considering V_O. Longer annealing time in the oxygen atmosphere might have reduced the V_O density. In the CZ900 thin film, a notable shift of 1.6 eV towards a higher BE value is observed in the O1s peak compared to CZ700. Three components were considered for the fitting: the O(iii) component centered at 531.8 eV is the signature of the Zn_2SiO_4 phase, which has been reported by Mier et al. [41]. The O(i) and O(ii) components indicate the presence of Cd − O and Zn−O bonding, respectively. Therefore, the presence of the Zn_2SiO_4 phase in CZ900 thin films is evidenced by the Si 2p, O 1 s, and Zn 2p core level spectra.

3.3.2. XANES at Zn $L_{3,2}$ edge

Fig. 5(a) shows the pre-, post-edge corrected, and normalized Zn $L_{2,3}$ edge XANES spectra for Z700, Z800, CZ700, CZ800, and CZ900 thin films. The feature **a1** around 1023 eV is a signature of the transition from Zn 2p to vacant Zn 4 s [44]. Features **a2** and **a3** are observed at 1027.8 and 1033 eV for 700 °C and 800 °C annealed thin films. Feature **a2** corresponds to the Zn $2p_{1/2} \rightarrow 3d$ antibonding transitions. The **a3** feature arises mainly due to the transition to an unoccupied s orbital in the conduction band (CB) [45].

The XRD and XPS analysis, indicate the presence of Zn_2SiO_4 along

with the transformed B2 phase, the change in electronic structure associated with the PT is probed with Zn $L_{3,2}$ edge. In Fig. 5(a) for CZ900 thin film, a sharp spike-like characteristic feature (**a4**) rises at 1023.5 eV. A broad hump-like feature appears in the CZ900 thin film at 1035.3 eV (**a5**) and 1050.4 eV (**a6**) instead of the valley-like feature of the CZ800 and CZ700 samples. Such spike-like characteristic feature has been reported to the willemite Zn_2SiO_4 phase by Becker et al. [46]. The Zn $L_{3,2}$ measurements were performed with surface sensitive TEY mode, indicating that the Zn_2SiO_4 nanoparticles have out-diffused from the film-substrate interface towards the surface of the thin film. From projected DOS calculation for the trigonal Zn_2SiO_4 phase, it has been observed that the valence band maxima (VBM) is formed mainly with hybridized O 2p and Zn 3d bands, and conduction band minima (CBM) is formed with Zn 4 s and Si 3p states [47]. Consequently, the formation of the Zn_2SiO_4 phase is not expected to cause any significant change in the VBM [47]. Thus, the **a4** feature at 1023.7 eV may be generated by the transition from Zn 2p to coupled Zn 4 s and Si 3p unoccupied states. In Fig. 5(b), we compare the experimental spectra Z700 and CZ900 with simulated Zn $L_{3,2}$ XANES spectra for a few possible structures. Comparing the experimental ZnO spectrum (Z700) with the calculated for wurtzite ZnO, we find very good agreement in peak positions and relative intensities, confirming the structural analysis by XRD and validating the theoretical approach. The experimental ZnO spectra are smoother than the theoretical ones, especially at high energy. This may be attributed to the fact that we have used a Lorentzian broadening of
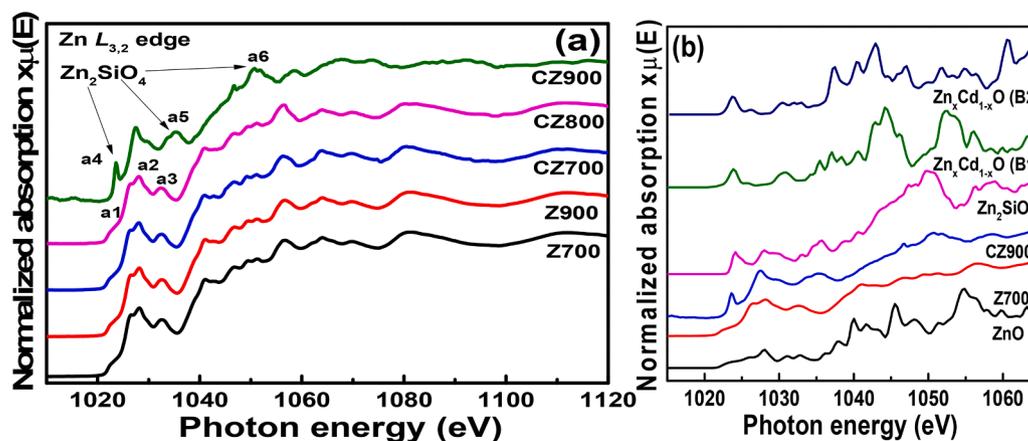
Fig. 5. (a): Zn $L_{3,2}$ XANES spectra for Z700, Z900, CZ700, CZ800 and CZ900 thin films; **(b)** Theoretical Zn $L_{3,2}$ XANES spectra for wurtzite ZnO, willemite Zn_2SiO_4 and $Zn_xCd_{1-x}O$ in B1 and B2 phases.

constant width, while energy-dependent self-energy effects, such as plasmon loss, are neglected. As possible structural candidates for the CZ900 film, we consider willemite Zn_2SiO_4 and $Zn_xCd_{1-x}O$ in the phases B1 and B2 with $x = 1/32$ and $x = 1/64$, respectively. We chose these low Zn concentrations because the B1 and B2 lattice structures observed in XRD (Fig. 1(a)) correspond to CdO rather than to cubic ZnO, which is unstable, implying that only a small amount of Zn can be incorporated into the CdO lattice. The calculated spectra of all three candidate structures reproduce the pronounced peak at threshold (1024 eV) in the experimental CZ900 spectrum. At higher energy, however, the theoretical spectra differ strongly. The Zn_2SiO_4 spectrum agrees remarkably well with CZ900 over the whole energy range. The $Zn_xCd_{1-x}O$ spectra (both B1 and B2), in contrast, differ strongly from the data, which is most clearly seen at energy 1045–1050 eV, where the CZ900 spectrum has a peak, while the $Zn_xCd_{1-x}O$ spectra have a dip. From this XANES analysis, we conclude that the local structure of the Zn ions in the CZ900 film is the same as in bulk Zn_2SiO_4, which proves the existence of the Zn_2SiO_4 phase in these films.

3.3.3. XANES at O K edge

Fig. 6 portrays the O *K* edge XANES data for Z700, Z900, CZ700, CZ800, and CZ900 thin films. The spectral features **b1** and **b2** between 531 and 537 eV are attributed to the electronic transitions from O 1 s to hybridized O 2*p* and non-localized Zn 4 s states. The sharp **b2** feature at 537 eV is due to the electronic transition to hybridized localized O 2p_z and 2p_{x+y} [48]. The absorption between 539 and 550 eV is caused by the transition to the hybridized O 2*p* and Zn 4*d* states. Beyond 550 eV, i.e., for the **b3** feature, electron transitions to hybridized O 2*p* and Zn 4*d* states are responsible for absorption [48]. We do not observe any significant change in b1, b2, and b3 features for Z700 and Z900 thin films. For CZ700 and CZ800 thin films, the overall spectral features are similar to features of Z700 and Z900 thin films. However, there is a slight intensity enhancement for CZ700 and CZ800 thin films compared to Z700 at b1 and b2 features. The transition to hybridized Cd 5 s and O 2*p* states also takes part in the absorption process, which might have increased the intensity. For the CZ900 thin film, the overall spectral feature has completely changed, and the intensity has also been reduced at the **b1** and **b2** regions. In the CZ900 thin film, evaporation of the CdO was observed from microscopy, which might have caused such intensity reduction. There is a 1.1 eV right-hand side shift in the inflection point of the absorption edge in CZ900 thin film compared to CZ700 thin film. Such a shift indicates a shift in the CBM towards higher energy [33]. CBM pinning can be considered direct evidence of changing band structure and possible PT [33].
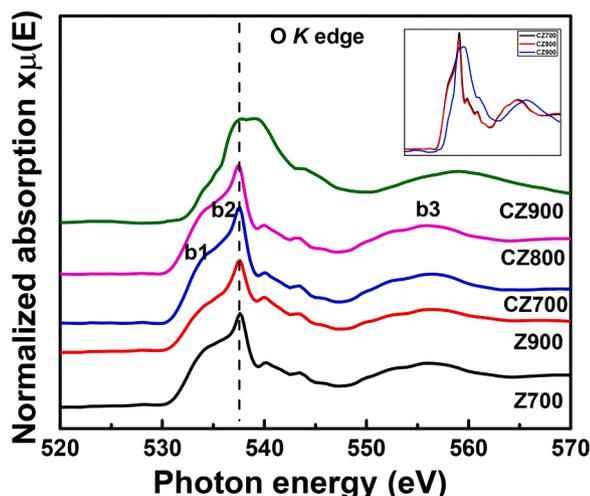
Fig. 6. O *K* XANES spectra for Z700, Z900, CZ700, CZ800 and CZ900 thin films.

3.3.4. K edge EXAFS

We have performed EXAFS modeling of Fourier transformed Zn *K* edge for Z700, Z900, CZ700, CZ800, and CZ900 thin films with Athena software package to determine the bond length around the photo-absorbing Zn atom and Debye-Waller factor (σ^2). We did not find significant changes in the local structure around the Zn atom between the different samples. This indicates that during the PT the Zn ions keep a tetrahedral ZnO_4 coordination, which is common for ZnO wurtzite and Zn_2SiO_4 willemite. This result rules out the possibility of substantial Cd substitution by Zn ions in the CdO sublattice during the PT, since this would generate octahedral ZnO_6 sites (for B1) or ZnO_8 sites (for B2) which would lead to observable changes in the EXAFS signal. Normalized Zn *K* edge data and the best fit for magnitude and real part of Fourier transformed $\chi(k).k^2$ spectra for all the thin films are shown in Figure S5(a, b) and S6(a, b) of SI. The details of the EXAFS fitting are mentioned in the SI file. The values of Zn−O and Zn − Zn bond lengths and σ^2 are shown in Table ST2.

3.4. Diffusion of Zn_2SiO_4 from film-substrate interface to surface observed with HAADF-STEM and TEM

STEM-EDX mapping for CZ900 thin film is shown in Fig. 7. Other STEM-EDX mapping for CZ900, CZ700 and Z900 thin films are shown in Figures S7, S8, and S9 of SI respectively. In Fig. 7, Zn comprised nanoparticles are non-uniformly embedded in a matrix containing Cd at the CZ900 thin film surface region. Element specific histograms at regions 1 and 3 in the bottom panel of Fig. 7 show the coexistence of Si, Zn, and O, i.e., indicating the possible formation of the Zn_2SiO_4 phase above the Si substrate. Si signal with 20 % atomic fraction is present beyond the 200 nm distance above the film-substrate interface in region 3 of Fig. 7. Similar amount of Si signal is absent above the film-substrate interface region in CZ700 and Z900 thin films. Even though the Zn_2SiO_4 phase is present in CZ700 and Z900 films, outward diffusion to the surface is found to be only possible in the CZ900 film. These findings are in line with previous reports on the formation of a zinc silicate phase in ZnO/Si heterostructures annealed at 900 °C, where orthorhombic $ZnSiO_3$ nanoparticles embedded in the amorphous interfacial layer were observed [49]. The thickness of Si oxide layer increases with increasing annealing temperature, giving rise to interdiffusion of Zn, Cd, O, and Si atoms. In Figure S8 for the CZ700 thin film, a SiO_x layer above the Si substrate is more prominent than in S9 for the Z900 thin film. This indicates that the presence of Cd supports the inter-diffusion at the film-substrate interface.

The cross-sectional TEM image in Fig. 8(a) shows a 5–30 nm thick SiO_x layer just above the Si substrate. The region inside the square box in Fig. 8(a) is shown at higher magnification in Fig. 8(b). Above the SiO_x layer, nanoparticles with Cd, Si, and O are present. From atomic fraction profile in Fig. 7, we can also observe the presence of Cd just above the Si substrate. Beyond this layer, Zn, Si, and O are observed, which confirms the possibility of Zn_2SiO_4 formation. The inter-planner spacing value determined from the lattice fringe in this layer is 0.41 nm, corresponding to the (3–11) planes of the willemite Zn_2SiO_4 phase [50].

3.5. Discussion of Pt mechanism and its thermodynamic aspects

In the $Cd_xZn_{1-x}O$ ($x = 0.4$) mixed binary oxide system, high-temperature annealing beyond 800 °C has caused a significant atomic inter-diffusion between the substrate and the film [49]. The notable diffusion of Si, starting at the film-substrate interface and further injection into the thin film layer, forms Si−O bonds. The thermal treatment at 900 °C annealing temperature enhances the thickness of the amorphous Si oxide layer caused by the interdiffusion of Si, O, Cd, and Zn atoms near the SiO_x layer [49]. However, the possible thermal interdiffusion was initiated with 800 °C annealing temperature. As we can observe from Fig. 1(a), B1 to B2 PT started from 800 °C. Therefore,
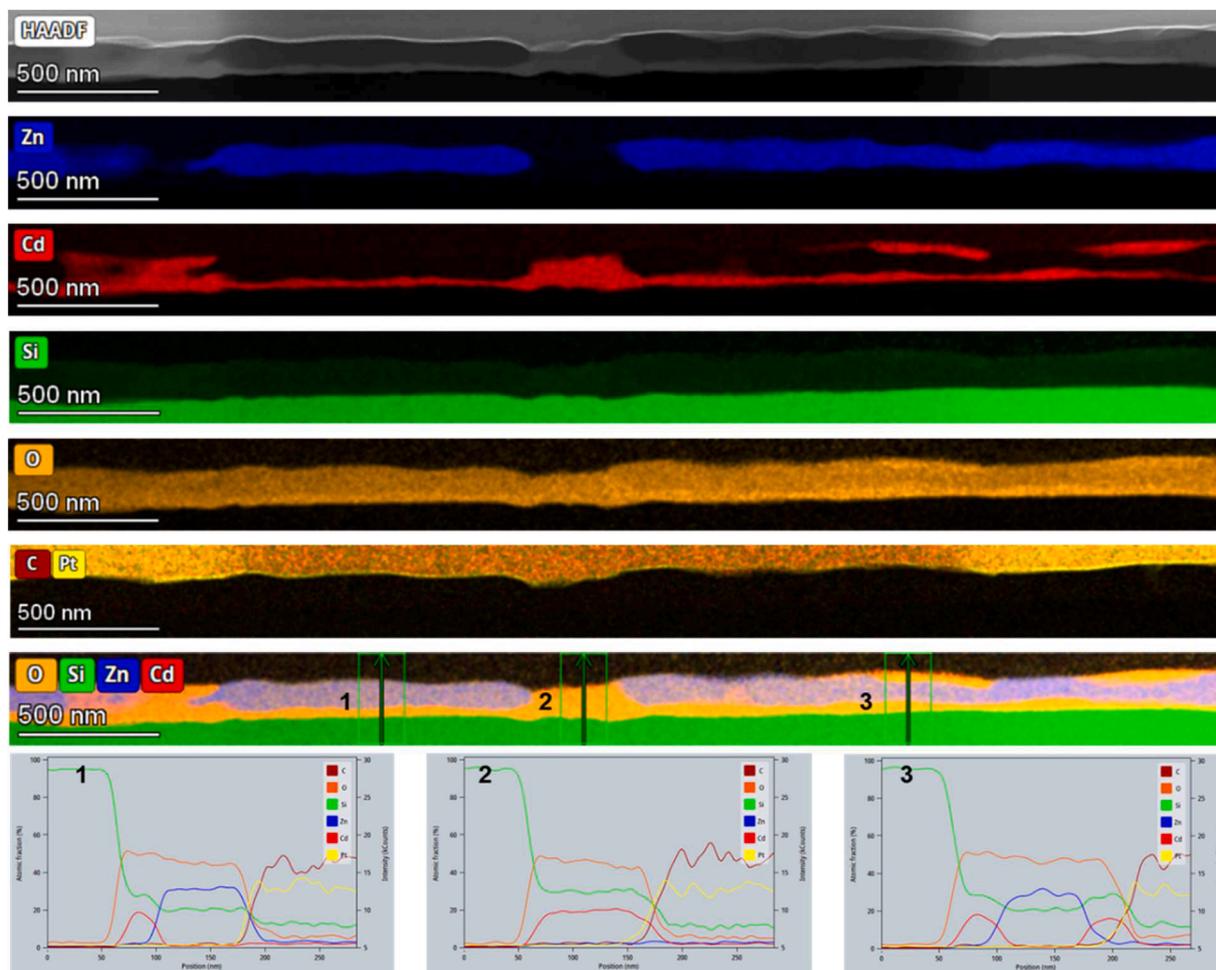
Fig. 7. Stacked HAADF-STEM image of CZ900 lamella at the top with elemental mapping at subsequent bottom layers. Atomic fraction profiles across the thin film are extracted for 3 different regions in the bottom panel.
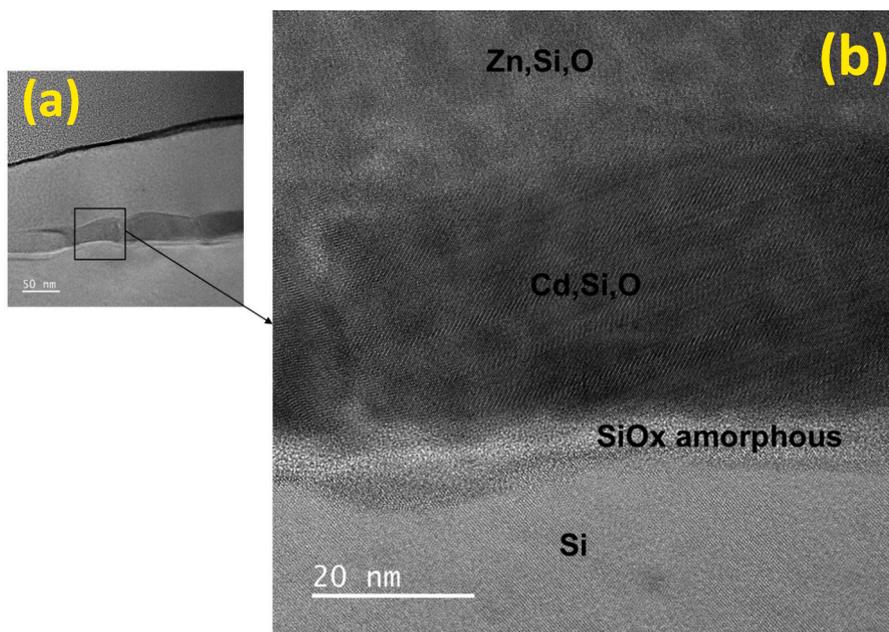
Fig. 8. (a) Cross-sectional TEM micrograph for CZ900 thin film; **(b)** The square boxed region in (a) has been shown in a magnified scale where atomic planes of the nanoparticles are visible.

the formation of Zn_2SiO_4 nanoparticles is anticipated to take place at 800 °C annealing temperature. Initially, an amorphous layer of $Zn_{2x}Si_{1-x}O_2$ is formed at the lower region of $Cd_xZn_{1-x}O$ thin film due to Si diffusion, and the width of this layer would possibly increase due to oxygen diffusion. This oxygen diffusion occurs near the Si substrate which further causes a deficiency in the $Zn_{2x}Si_{1-x}O_2$ layer. Adjustment of the stoichiometry embeds the trigonal Zn_2SiO_4 nanoparticles in the $Zn_{2x}Si_{1-x}O_2$ interface layer between thin film and Si substrate, which can provide oxygen for the $Zn_{2x}Si_{1-x}O_2$ interface layer [49]. Further, one hour of annealing at 900 °C temperature provides sufficient energy to the system, resulting in an outward diffusion of the trigonal Zn_2SiO_4 nanoparticles toward the thin film surface. The formation of Zn_2SiO_4 in the ZnO/Si heterostructure and subsequent diffusion towards the film surface is well reported by Xu et al. [51]. At 900 °C, possible evaporation of CdO nanoparticles from the thin film supports the outward diffusion of Zn_2SiO_4 nanoparticles, further minimizing the surface energy [33]. As rhombohedral Zn_2SiO_4 has a larger unit cell volume, it will, expectedly, produce compressional stress upon both CdO and ZnO sublattice. The unit cell volume for ZnO wurtzite, CdO rocksalt, and Zn_2SiO_4 rhombohedral lattice systems are 47.40 Å^3, 105.29 Å^3, 1569.22 Å^3, respectively. At 900 °C temperature, outward diffusion of Zn_2SiO_4 nanoparticles with sufficient thermal energy exerts pressure upon the CdO sublattice and achieves a thermodynamically stable B2 phase. The local pressure exerted by the Zn_2SiO_4 lattice is enough to trigger PT in the CdO sublattice due to lower P_{TC} (89 GPa). However, the same cannot change the phase in ZnO due to higher P_{TC} (256 Gpa). Zn_2SiO_4 phase formation at film-substrate interface is expected for Z900 thin film, but we do not observe the trace of Zn_2SiO_4 at the surface with XPS and XAS. This brings us to the conclusion that Cd incorporation in ZnO matrix supports the outward diffusion Zn_2SiO_4 which is not found to be possible only for ZnO. Such trigonal Zn_2SiO_4 has caused a mixed phase formation from hexagonal ZnO to a mixture of hexagonal plus trigonal mixed phase at 800 °C annealing temperature for ZnO/Si heterostructure [52]. The enthalpy difference (ΔH) in the PT process can be subdivided into two contributions, i.e., pressure term (ΔPV) and internal energy change (ΔU). B1 to B2 PT can occur if ΔPV becomes more negative than positive ΔU, which is the barrier energy for stabilizing the B1 phase. The enhanced local pressure from the Zn_2SiO_4 lattice causes ΔPV to be more negative with a compressed CdO sublattice than positive ΔU, further triggering the PT. Apart from CsCl, as per ab initio calculations, there are possibly many high-pressure phases for CdO, such as NiAs, Zinc blende, wurtzite, etc. The intermediate phase is observed in the pathway between B1 to B2 PT for some TMOs. In the present scenario, we did not observe any other intermediate phase during B1 to B2 PT for CdO. Being the end member, Cd is similar to the IIA group element with $[Kr]4d^{10}5s^2$ ground state electronic configuration. The filled 4d level might be the reason for its different behavior from other TMOs and similar to the IIA-VIA family of oxides such as CaO, SrO, and BaO among others [53].

To illustrate the bonding character and description of orbital hybridization with changing Cd concentration, the partial density of states (PDOS) is calculated from ZnO to CdO supercell using GGA. The PDOS is displayed in Figure S10(a, b, c, d, and e). PDOS calculation has shown that the VB in wurtzite ZnO is dominated by Zn 3d and O 2p states (Figure S10(a)). At the top of the VB, Zn 3d levels are hybridized with O 2p levels. In VB from −4 to −6 eV, PDOS is dominated by Zn 3d core states where O 2p states are absent. From the top of the VB, i.e., from 0 to −4 eV, mainly Zn 3d and O 2p hybridized states are present. In Figure S10(e), for Rocksalt CdO, the top of the VB is constructed with the O 2p states. The hybridized O 2p and Cd 4d states are confined within −3 to −4 eV below the VBM. In our earlier work, temperature-mediated Rocksalt to wurtzite phase transformation (PT) in CdO thin film has been reported where the VBM has shifted from zone boundary to zone center with PT [33]. So, with such Cd concentration in the ZnO matrix, we remark that the system is on the verge of triggering a structural PT with the possible external influence of change in external

pressure/annealing temperature. In a nutshell, the tetrahedral coordination allows the presence of O 2p – Zn 3d repulsive interaction throughout the BZ. In contrast, octahedral coordination in CdO with inversion symmetry doesn't allow Cd 4d–O 2p repulsive interaction at Γ point, causing shifting of VBM away from the Γ point [20,54]. Such p-d repulsive interaction is potentially the origin of anomalous VB structure for IIB-VIA compounds with Rocksalt structure. IIB-VIA compounds with strong p-d repulsion are prone to structural PT as d orbital in the upper VB triggers the anomalous dispersion making the system less stable. Increasing Cd concentration ($\sim$ 50 %), the system becomes prone to PT in the presence of local pressure [55].

4. Conclusion

In conclusion, high temperature-driven B1 to B2 structural PT in $Cd_xZn_{1-x}O$ ($x = 0.4$) has been reported. X-ray diffractograms and complementary Raman spectroscopic results revealed the evolution of the B2 phase with thermal annealing from $\sim$700 °C to $\sim$900 °C. In addition, microscopic observations reflect grain growth, followed by agglomeration of grains and void formation with increasing annealing temperature. The formation of willemite Zn_2SiO_4 at the film and substrate interface and its further out-diffusion with increasing annealing temperature has caused a local pressure generation inside the lattice triggering the PT. Core level spectroscopies XPS, XANES, HAADF-STEM, and cross-sectional TEM techniques have evidenced the presence and distribution of willemite Zn_2SiO_4 nanoparticles in a thin film matrix. This study reports the first instance of a B1 to B2 phase transition induced by local pressure in a solgel-derived $Cd_xZn_{1-x}O$ ($x = 0.4$) thin film. We will further investigate other Cd concentrations to evaluate the possibility of a transformed B2 phase.

Declaration of competing interest

The authors declare that they have no known competing financial interests or personal relationships that could have appeared to influence the work reported in this paper.

Acknowledgment

Supplementary materials

Supplementary material associated with this article can be found, in the online version, at doi:10.1016/j.actamat.2024.119744.

References

[1] J.de O. Primo, J.de S. Correa, D.F.L. Horsth, A. Das, M. Zając, P. Umek, R. Wattiez, F.J. Anaissi, R.C.A. Onderwater, C. Bittencourt, Antiviral properties against SARS-CoV-2 of nanostructured ZnO obtained by green combustion synthesis and coated in waterborne acrylic coatings, Nanomaterials 12 (2022) 4345.

[2] R. Serhane, S. Abdelli-Messaci, S. Lafane, H. Khales, W. Aouimeur, A. Hassein-Bey, T. Boutkedjirt, Pulsed laser deposition of piezoelectric ZnO thin films for bulk acoustic wave devices, Appl. Surf. Sci. 288 (2014) 572–578.

[3] B. Bhat, S. Chakraborty, Acoustic-wave-induced analyte separation in narrow fluidic confinements in the presence of interfacial interactions, Langmuir. 26 (2010) 15035–15043.

[4] S. Agarwal, P. Rai, E.N. Gatell, E. Llobet, F. Güell, M. Kumar, K. Awasthi, Gas sensing properties of ZnO nanostructures (flowers/rods) synthesized by hydrothermal method, Sens. Actuators. B Chem. 292 (2019) 24–31.

[5] K.M. Yu, M.A. Mayer, D.T. Speaks, H. He, R. Zhao, L. Hsu, S.S. Mao, E.E. Haller, W. Walukiewicz, Ideal transparent conductors for full spectrum photovoltaics, J. Appl. Phys. 111 (2012).

[6] Y. Yang, S. Jin, J.E. Medvedeva, J.R. Ireland, A.W. Metz, J. Ni, M.C. Hersam, A. J. Freeman, T.J. Marks, CdO as the archetypical transparent conducting oxide. Systematics of dopant ionic radius and electronic structure effects on charge transport and band structure, J. Am. Chem. Soc. 127 (2005) 8796–8804.

[7] M. Yan, M. Lane, C.R. Kannewurf, R.P.H. Chang, Highly conductive epitaxial CdO thin films prepared by pulsed laser deposition, Appl. Phys. Lett. 78 (2001) 2342–2344.

[8] Y. Chen, S. Zhang, W. Gao, F. Ke, J. Yan, B. Saha, C. Ko, J. Suh, B. Chen, J. W. Ager III, Pressure-induced structural transition of CdxZn1− xO alloys, Appl. Phys. Lett. 108 (2016) 152105.

[9] A. Janotti, C.G. Van de Walle, Fundamentals of zinc oxide as a semiconductor, Rep. Progr. Phys. 72 (2009) 126501.

[10] A. Schleife, C. Rödl, J. Furthmüller, F. Bechstedt, Electronic and optical properties of MgxZn1− xO and CdxZn1− xO from ab initio calculations, New. J. Phys. 13 (2011) 085012.

[11] T. Makino, Y. Segawa, M. Kawasaki, A. Ohtomo, R. Shiroki, K. Tamura, T. Yasuda, H. Koinuma, Band gap engineering based on Mg x Zn 1− x O and Cd y Zn 1− y O ternary alloy films, Appl. Phys. Lett. 78 (2001) 1237–1239.

[12] V. Venkatachalapathy, A. Galeckas, M. Trunk, T. Zhang, A. Azarov, A.Y. Kuznetsov, Understanding phase separation in ZnCdO by a combination of structural and optical analysis, Phys. Rev. B 83 (2011) 125315.

[13] A. Schleife, M. Eisenacher, C. Rödl, F. Fuchs, J. Furthmüller, F. Bechstedt, Ab initio description of heterostructural alloys: thermodynamic and structural properties of Mg x Zn 1− x O and Cd x Zn 1− x O, Phys. Rev. B 81 (2010) 245210.

[14] J. Ishihara, A. Nakamura, S. Shigemori, T. Aoki, J. Temmyo, Zn1− xCdxO systems with visible band gaps, Appl. Phys. Lett. 89 (2006).

[15] T. Ohashi, K. Yamamoto, A. Nakamura, T. Aoki, J. Temmyo, Optical properties of wurtzite Zn1-xCdxO films grown by remote-plasma-enhanced metalorganic chemical vapor deposition, Jpn. J. Appl. Phys. 46 (2007) 2516.

[16] D.M. Detert, S.H.M. Lim, K. Tom, A.V. Luce, A. Anders, O.D. Dubon, K.M. Yu, W. Walukiewicz, Crystal structure and properties of CdxZn1− xO alloys across the full composition range, Appl. Phys. Lett. 102 (2013).

[17] X. Ma, P. Chen, R. Zhang, D. Yang, Optical properties of sputtered hexagonal CdZnO films with band gap energies from 1.8 to 3.3eV, J. Alloys. Compd. 509 (2011) 6599–6602.

[18] H. Liu, H. Mao, M. Somayazulu, Y. Ding, Y. Meng, D. Häusermann, B 1-to-B 2 phase transition of transition-metal monoxide CdO under strong compression, Phys. Rev. B 70 (2004) 094114.

[19] J.E. Jaffe, J.A. Snyder, Z. Lin, A.C. Hess, LDA and GGA calculations for high-pressure phase transitions in ZnO and MgO, Phys. Rev. B 62 (2000) 1660.

[20] R.J. Guerrero-Moreno, N. Takeuchi, First principles calculations of the ground-state properties and structural phase transformation in CdO, Phys. Rev. B 66 (2002) 205205.

[21] A.N. Baranov, P.S. Sokolov, V.A. Tafeenko, C. Lathe, Y. v Zubavichus, A. A. Veligzhanin, M. v Chukichev, V.L. Solozhenko, Nanocrystallinity as a route to metastable phases: rock salt ZnO, Chem. Mater. 25 (2013) 1775–1782.

[22] N. Gautam, F. Singh, S.K. Gautam, R.G. Singh, S. Ojha, A. Kapoor, Growth of highly transparent CdxZn1−xO (CZO) thin films: structural and optical studies, J. Alloys. Compd. 650 (2015) 311–317, https://doi.org/10.1016/j.jallcom.2015.07.283.

[23] M. Zając, T. Giela, K. Freindl, K. Kollbek, J. Korecki, E. Madej, K. Pitala, A. Kozioł-Rachwał, M. Sikora, N. Spiridis, The first experimental results from the 04BM (PEEM/XAS) beamline at Solaris, Nucl. Instrum. Methods Phys. Res. B 492 (2021) 43–48.

[24] J. Szlachetko, J. Szade, E. Beyer, W. Błachucki, P. Ciochoń, P. Dumas, K. Freindl, G. Gazdowicz, S. Glatt, K. Guła, SOLARIS national synchrotron radiation centre in Krakow, Poland, Euro. Phys. J. Plus 138 (2023) 1–10.

[25] J.P. Perdew, M. Ernzerhof, K. Burke, Rationale for mixing exact exchange with density functional approximations, J. Chem. Phys. 105 (1996) 9982–9985.

[26] K. Mathew, R. Sundararaman, K. Letchworth-Weaver, T.A. Arias, R.G. Hennig, Implicit solvation model for density-functional study of nanocrystal surfaces and reaction pathways, J. Chem. Phys. 140 (2014) 084106.

[27] H.J. Monkhorst, J.D. Pack, Special points for Brillouin-zone integrations, Phys. Rev. B 13 (1976) 5188.

[28] E. Péan, J. Vidal, S. Jobic, C. Latouche, Presentation of the PyDEF post-treatment Python software to compute publishable charts for defect energy formation, Chem. Phys. Lett. 671 (2017) 124–130.

[29] A. Stoliaroff, S. Jobic, C. Latouche, PyDEF 2.0: an easy to use post-treatment software featuring a graphical user interface, J. Comput. Chem. 39 (2018) 2251–2261.

[30] Y. Caglar, M. Caglar, S. Ilican, A. Ates, Morphological, optical and electrical properties of CdZnO films prepared by sol–gel method, J. Phys. D. Appl. Phys. 42 (2009) 65421.

[31] A. Singh, D. Kumar, P.K. Khanna, A. Kumar, M. Kumar, Dielectric anomaly in Mg doped ZnO thin film deposited by Sol–Gel method, J. Electrochem. Soc. 158 (2010) G9.

[32] W.J. Lee, Y.H. Chang, Growth without postannealing of monoclinic VO2 thin film by atomic layer deposition using VCl4 as precursor, Coatings 8 (2018) 431.

[33] A. Das, C.P. Saini, D. Singh, R. Ahuja, A. Kaur, S. Aliukov, D. Shukla, F. Singh, High temperature-mediated rocksalt to wurtzite phase transformation in cadmium oxide nanosheets and its theoretical evidence, Nanoscale 11 (2019) 14802–14819.

[34] S.S. Brenner, G.W. Sears, Mechanism of whisker growth—III nature of growth sites, Acta Metallurgica 4 (1956) 268–270.

[35] A. Das, D. Singh, C.P. Saini, R. Ahuja, A. Kaur, S. Aliukov, Orbital hybridization-induced band offset phenomena in Ni x Cd 1− x O thin films, Nanoscale 12 (2020) 669–686.

[36] G. Moretti, Auger parameter and Wagner plot in the characterization of chemical states by X-ray photoelectron spectroscopy: a review, J. Electron. Spectros. Relat. Phenomena 95 (1998) 95–144.

[37] R. Mu, A. Steigert, N. Lin, R. Wilks, M. Bär, Y. Zhang, The chemical structure of the ZnO/SiC heterointerface as revealed by electron spectroscopies, J. Phys. D. Appl. Phys. 48 (2015) 305304.

[38] L.S. Dake, D.R. Baer, J.M. Zachara, Auger parameter measurements of zinc compounds relevant to zinc transport in the environment, Surf. Interface Anal. 14 (1989) 71–75.

[39] J.G. Ma, Y.C. Liu, C.S. Xu, Y.X. Liu, C.L. Shao, H.Y. Xu, J.Y. Zhang, Y.M. Lu, D. Z. Shen, X.W. Fan, Preparation and characterization of ZnO particles embedded in Si O 2 matrix by reactive magnetron sputtering, J. Appl. Phys. 97 (2005) 103509.

[40] D. Gerlach, M. Wimmer, R.G. Wilks, R. Félix, F. Kronast, F. Ruske, M. Bär, The complex interface chemistry of thin-film silicon/zinc oxide solar cell structures, Phys. Chem. Chem. Phys. 16 (2014) 26266–26272.

[41] U. Meier, C. Pettenkofer, Morphology of the Si–ZnO interface, Appl. Surf. Sci. 252 (2005) 1139–1146.

[42] A. Kaur, D. Singh, A. Das, K. Asokan, C.L. Chen, I.B. Mishra, R. Ahuja, Spin and valence variation in cobalt doped barium strontium titanate ceramics, Phys. Chem. Chem. Phys. 24 (2022) 19865–19881.

[43] G. Dasi, T. Lavanya, S. Suneetha, S. Vijayakumar, J.J. Shim, K. Thangaraju, Raman and X-ray photoelectron spectroscopic investigation of solution processed Alq3/ ZnO hybrid thin films, Spectrochim. Acta a Mol. Biomol. Spectrosc. 265 (2022) 120377.

[44] J.W. Chiou, K.P.K. Kumar, J.C. Jan, H.M. Tsai, C.W. Bao, W.F. Pong, F.Z. Chien, M. H. Tsai, I.H. Hong, R. Klauser, Diameter dependence of the electronic structure of ZnO nanorods determined by x-ray absorption spectroscopy and scanning photoelectron microscopy, Appl. Phys. Lett. 85 (2004) 3220–3222.

[45] M.W. Murphy, W.R. Diebel, Y.M. Yiu, T.K. Sham, Cr doped ZnO nanostructures: synthesis, electronic structures, and magnetic properties, Can. J. Chem. 95 (2017) 1225–1232.

[46] C. Becker, M. Pagels, C. Zachäus, B. Pollakowski, B. Beckhoff, B. Kanngießer, B. Rech, Chemical speciation at buried interfaces in high-temperature processed polycrystalline silicon thin-film solar cells on ZnO: al, J. Appl. Phys. 113 (2013) 044519.

[47] S.Z. Karazhanov, P. Ravindran, H. Fjellvåg, B.G. Svensson, Electronic structure and optical properties of ZnSiO 3 and Zn 2 SiO 4, J. Appl. Phys. 106 (2009) 123701.

[48] S. Krishnamurthy, C. McGuinness, L.S. Dorneles, M. Venkatesan, J.M.D. Coey, J. G. Lunney, C.H. Patterson, K.E. Smith, T. Learmonth, P.A. Glans, Soft-x-ray spectroscopic investigation of ferromagnetic Co-doped ZnO, J. Appl. Phys. 99 (2006) 08M111.

[49] J.M. Yuk, J.Y. Lee, J.H. Jung, D.U. Lee, T.W. Kim, D.I. Son, W.K. Choi, Formation mechanism of Zn Si O 3 nanoparticles embedded in an amorphous interfacial layer between a ZnO thin film and an n-Si (001) substrate due to thermal treatment, J. Appl. Phys. 103 (2008) 083520.

[50] A. Das, C. Balasubramanian, P. Orpe, G.M. Pugliese, A. Puri, A. Marcelli, N.L. Saini, Morphological, electronic, and magnetic properties of multicomponent cobalt oxide nanoparticles synthesized by high temperature arc plasma, Nanotechnology. 33 (2021) 095603.

[51] X. Xu, P. Wang, Z. Qi, H. Ming, J. Xu, H. Liu, C. Shi, G. Lu, W. Ge, Formation mechanism of Zn2SiO4 crystal and amorphous SiO2 in ZnO/Si system, J. Phys. Condens. Matter 15 (2003) L607.

[52] X. Xu, C. Guo, Z. Qi, H. Liu, J. Xu, C. Shi, C. Chong, W. Huang, Y. Zhou, C. Xu, Annealing effect for surface morphology and luminescence of ZnO film on silicon, Chem. Phys. Lett. 364 (2002) 57–63.

[53] P. Toledano, K. Knorr, L. Ehm, W. Depmeier, Phenomenological theory of the reconstructive phase transition between the NaCl and CsCl structure types, Phys. Rev. B 67 (2003) 144106.

[54] J.E. Jaffe, R. Pandey, A.B. Kunz, Electronic structure of the rocksalt-structure semiconductors ZnO and CdO, Phys. Rev. B 43 (1991) 14030.

[55] Y. Chen, S. Zhang, W. Gao, F. Ke, J. Yan, B. Saha, C. Ko, J. Suh, B. Chen, J.W. Ager, Pressure-induced structural transition of CdxZn1− xO alloys, Appl. Phys. Lett. 108 (2016).